Quantum Accurate Prediction of Plutonium–Plutonium Dihydride Phase Equilibrium Using a Spin-Lattice Model

Ryan Gotchy Mullen* and Nir Goldman

Physical and Life Sciences Directorate, Lawrence Livermore National Laboratory, Livermore, CA 94550 USA

E-mail: mullen10@llnl.gov

Abstract

Plutonium-based materials are vital for use as nuclear fuels and as portable power sources for space vehicles. However, elucidating their sensitivity to hydriding corrosion represents an extreme challenge due to the toxicity of Pu as well as its anomalous magnetic properties. In this work, we develop a spin-lattice model of plutonium–plutonium dihydride ($Pu–PuH_2$) phase equilibrium that retains the accuracy of density functional theory (DFT) while yielding many orders of magnitude improvement in computational efficiency. Using Monte Carlo and free energy sampling algorithms, we compute a number of $Pu–PuH_2$ equilibrium properties that are difficult to probe experimentally, including equilibrium pressures and phase compositions at room temperature and the PuH_2 heat of formation. Our method will have particular impact on these types of materials studies, where there is a strong need for computationally efficient approaches to bridge time and length scale gaps between quantum calculations and experiments.

Graphical TOC Entry
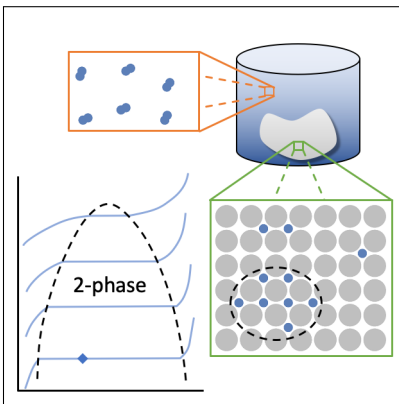
The unique material properties of plutonium make it a possible source of heat to generate steam in power production or to power radioisotope thermoelectric generators for space probes and, once upon a time, in pacemakers.[1] However, even trace amounts of hydrogen gas or water vapor dissociatively absorb in plutonium due to the high inherent reactivity of the metal. Above a temperature-dependent solubility limit, the absorbed H atoms aggregate to form plutonium dihydride (PuH_2) flakes or powder.[2] Plutonium hydride can further catalyze rapid, catastrophic oxidation or induce pyrophoricity,[3] generating toxic waste. As a result, understanding plutonium corrosion properties is of primary importance for its continued use in many application areas.

The complexities of plutonium hydriding can be illustrated by a comparison to hydriding in a more common metal, such as palladium. The critical temperature of the palladium–palladium hydride phase envelope is 550 K (277°C), well below the palladium metal melting temperature of 1828 K (1555°C).[4] In contrast, the critical temperature of the plutonium–plutonium dihydride (Pu–PuH_2) phase envelope is unknown exactly, but it has been shown that PuH_2 will crystallize from the melt when liquid plutonium at 1023 K (800°C), 160 K above the plutonium melting point, is exposed to hydrogen.[5] In addition, hydriding in face-centered cubic (fcc) δ-Pu (of interest for engineering applications due to its high ductility[6]) induces a large volume expansion of ∼60%, compared to an expansion of only ∼10% in palladium hydriding, resulting in flaking and the complete degradation of Pu-based materials due to this lattice mismatch. Finally, neutron diffraction reveals that H atoms randomly occupy interstitial octahedral (O) sites in palladium hydride.[7] In contrast, no neutron diffraction studies have been performed on δ-Pu or PuH_2 to indicate how H atoms partition between O sites and tetrahedral (T) sites, though investigations of lanthanide-hydrides show that O sites are not occupied until all available T sites are filled.[8]

Conducting experiments with plutonium is exceedingly difficult due to its toxicity and radioactivity. The lowest temperature at which the composition of the PuH_2 phase has been reported is 773 K (500°C).[5] Mulford and Sturdy additionally reported equilibrium

3

pressures at 673 and 723 K (400 and 450°C) but were unable to determine the equilibrium compositions at these temperatures, reporting that it took 20 hours to equilibrate at each trial composition. Allen[9] and Richmond et al.[10] both published equilibrium pressures, but only determined the lower solubility limit of H in Ga-stabilized δ-Pu, not the upper limit in the PuH_2 phase. Allen's lowest temperature data was taken at 748 K (475°C). Richmond et al. reported results as low as 623 K (350°C) and allowed 60 hours for equilibration.

This scarcity of experimental data for bulk plutonium hydriding makes computer model prediction particularly attractive for possible chemical and environmental studies. Recent efforts have utilized density functional theory (DFT) to assess the crystal structure, density, magnetization, conductivity, elasticity, and reactivity of plutonium[11–18] and plutonium hydrides.[19–22] These properties were computed from energy-minimized configurations at 0 K, which excludes potentially important thermal effects on the free energy as a function of composition. Many molecular simulation methods have been developed for sampling free energies, including umbrella sampling,[23] alchemical transformations,[24–26] adaptive biasing,[27] and flat histogram methods.[28,29] These methods generally require millions of force evaluations, and calculations of statistically independent dynamic trajectories. In contrast, DFT calculations on δ-Pu can require hundreds of thousands of CPU hours for the simulation of sub-ps molecular dynamics trajectories on small systems.[30] As a result, there exists a great need for computational approaches for these materials that can yield many orders of magnitude increase in computational efficiency while retaining the accuracy of DFT.

Spin-lattice models are an attractive alternative for phase diagram calculations due to their inherent simplicity and reduced order, allowing for substantial savings in computational expense.[31,32] They can exhibit linear scaling and are significantly more efficient than classical force fields or semi-empirical quantum models. They are also much easier to train to fitting data because they require only a small number of parameters. They are particularly attractive for bulk Pu/H phase diagram modeling, where hydrogen atoms are restricted to occupy only either O or T sites. As a result, a spin lattice model for hydriding can be

determined from small DFT datasets, which is highly advantageous for computationally dif-
ficult systems such as actinides. Lattice models have been previously developed to model
hydrogen diffusion in palladium alloys[33–38] and in nickel alloys.[39] These models predict the H
absorption energy as a function of the local metallic composition. However, H–H interactions
are neglected in these studies, limiting them to dilute H concentrations. In this work, we
develop a novel spin-lattice model for Pu–PuH$_2$ phase equilibria. Our model incorporates
H–H interactions in the concentrated hydrogen limit, allowing for simulation of experiments
on both hydrogen-poor and hydrogen-rich plutonium phases for the first time.

The Hamiltonian of a PuH$_x$ spin-lattice in the grand canonical ensemble is

$$H = E^{config} + F^{vib} + \frac{\mu_{H_2}}{2} N_H \tag{1}$$

where the configurational potential energy E^{config}, the vibrational free energy F^{vib}, and
number of hydrogen atoms N_H are properties of the microstate, while the chemical poten-
tial of a gas-phase hydrogen molecule μ_{H_2}, the number of plutonium atoms N_{Pu}, and the
temperature T are held constant. Each absorbed H is treated as an independent quantum
harmonic oscillator. Consequently, Eq. 1 contains the analytic free energy F^{vib} rather than
a potential energy E^{vib} and corresponding quantum degrees of freedom. A $P\Delta V$ term for H
in the Pu lattice is not included in Eq. 1 because under the conditions studied here its value
is several orders of magnitude smaller than other terms. The impact of plutonium defects
on Pu–PuH$_2$ equilibrium are not considered in this work.

The configurational potential energy E^{config} accounts for the arrangement adopted by
the N_H absorbed hydrogens. In the δ-Pu phase, we anticipate this will mostly consist of
isolated H atoms in O or T sites. In the PuH$_2$ phase, stoichiometry suggests that H atoms
predominantly occupy T sites, though with possible T-site vacancies and O-site interstitials.
Small clusters of aggregated H atoms and multi-phase configurations will additionally in-
troduce a strain or interfacial energy arising from the lattice mismatch between the δ-Pu

and PuH$_2$ regions. Computing the DFT energy of such configurations would require especially large supercells such that the Pu atoms at the boundaries of the cell have zero strain. Alternatively, the strain energy could be accounted for analytically using idealized models of, for example, spheroidal or cubical nuclei.[40,41] Since our primary goal is to sample the equilibrium properties of the Pu–PuH$_2$ phase envelope, the details of the transition between phases are unimportant and we choose the simplest option, viz., to neglect strain effects in our calculations altogether.

Due to the likely strong screening effects of the intervening plutonium atoms, we parameterize H–H interaction energies between nearest neighbor sites only. This results in three types of H–H energies: those between hydrogens in neighboring T sites (TT), those in neighboring O sites (OO), and cross interactions (OT). Consequently, E^{TT}, E^{OT}, and E^{OO} are determined by reference to a dataset of DFT energies computed using VASP.[42–44] Eight PuH$_x$ configurations with $N_{Pu} = 32$ and variable N_H were optimized using a plane-wave cutoff of 500 eV, spin-polarized plutonium ions, and the GGA+U approach of Dudarev et al.[45] to model f-electron correlations. Fig. 1a shows one such configuration (1) and two reference configurations (0, H2) that were used to compute the change in energy from inserting an additional hydrogen atom. For example, the absorption energy of H in an isolated O site is $E^{OO}(0) = E_1 - E_0 - E_H$, where E_1 is the DFT energy of optimized configuration 1, E_0 is the reference energy of plutonium supercell with no hydrogens, and E_H is the reference energy of a hydrogen atom (see Eq. S2 and supporting information for more details). As shown in Fig. 1b, if an isolated hydrogen atom moves from an O site to a T site, the energy increases by 20 kJ/mol. Similarly, the energy increases by 24-32 kJ/mol if a pair of isolated hydrogen atoms move into neighboring sites, suggesting that there is an energetic barrier to hydride nucleation. However, there is also an energetic driving force to forming a hydride phase. Once all six neighboring T sites are occupied, the energy for occupying the central T site is 37 kJ/mol lower than occupying an isolated T site. As with the strain energy, the potential energies of intermediate H clusters and multi-phase configurations do not contribute to

6

any calculated equilibrium properties. We determine the absorption energies of H atoms in these intermediate configurations by linearly interpolation, as shown in Fig. 1b. As will be shown, all OO and OT interactions are sufficiently energetically prohibitive as to be rare in either δ-Pu or PuH$_2$ phases. In addition, we simplify our tabulated energies by ignoring OO interactions when OT interactions are present since the OT energies are significantly more repulsive that those from OO.

Accordingly, the configurational potential energy E^{config} can be written as:

$$E^{config} = \sum_{i \in T} n_i E^{TT}(N_i^T) + \sum_{i \in O} n_i \left[\theta(N_i^T - 1) E^{OT}(N_i^T) + \theta(-N_i^T) E^{OO}(N_i^O) \right] \qquad (2)$$

where n_i is 1 if site i is occupied and 0 otherwise, and the function E^{OT} accounts for H–H interactions between a hydrogen in an O site and the N_i^T hydrogens in the nearest neighbor T sites. E^{TT}, E^{OO}, and N_i^O are defined similarly. The first sum is over T sites, the second sum is over O sites, and the Heaviside function $\theta(n)$ is 1 if $n \geq 0$ and 0 otherwise.
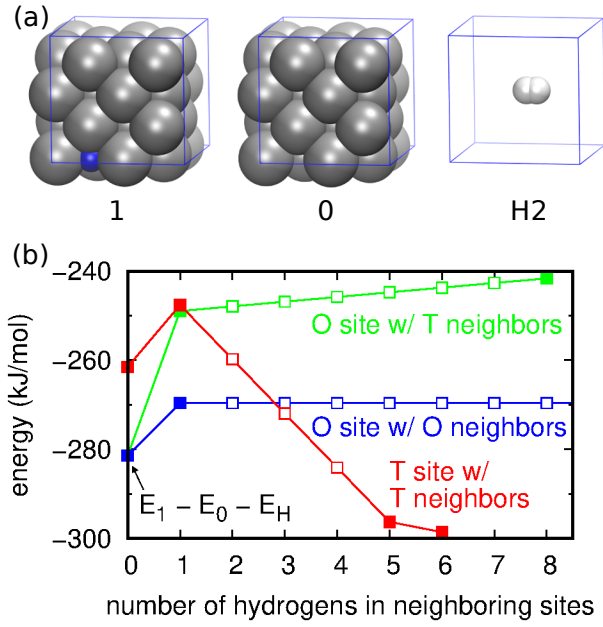
Figure 1: (a) Snapshots of DFT-optimized configurations 1, 0, and H2, corresponding to plutonium with one occupied O site, pure δ-Pu, and an isolated hydrogen molecule. (b) Change in potential energy for inserting a hydrogen into a site with the specified number of occupied neighboring sites. Filled symbols indicate parameters computed from DFT energies, while open symbols were determined from linear interpolation.

Zero-point energies and entropic contributions from the vibration of light interstitials such as H in metals can be significant. These off-lattice contributions are included analytically. We computed the normal mode vibrational frequencies ω_{ij} for a hydrogen in site i along normal mode j via DFT using finite displacement. The resulting spectrum (see Fig. S2) shows that the plutonium and hydrogen vibrational modes differ greatly in frequency. Moreover, the plutonium vibrational frequencies in PuH_2 are shifted by only a few wavenumbers relative to pure δ-Pu so the contributions of these modes to differences in the energy are negligible. Inserting a hydrogen atom, on the other hand, creates three vibrational modes that did not exist in the previous configuration. These modes are treated as quantum harmonic oscillators, with the following analytical free energy expression:

$$F^{vib} = \sum_i n_i \sum_j \left(\frac{k_B \Theta_{ij}}{2} + k_B T \ln(1 - e^{-\Theta_{ij}/T}) \right). \tag{3}$$

Here, Θ_{ij} is the vibrational temperature $\hbar\omega_{ij}/k_B$. The frequencies ω_{ij} of a hydrogen atom in an O site and in a T site in both the δ-Pu and PuH_2 phases are given in Table S5. H atoms vibrate at lower frequencies in the larger O sites than in the smaller T sites. Similarly, H atoms vibrate at lower frequencies in PuH_2 than in δ-Pu, due to the larger unit cell of the former.

The Pu–PuH_2 equilbirium chemical potential was computed by sampling the free energy using the Wang-Landau (WL) algorithm[28] to drive the simulation away from previously visited regions of configuration space. We first attempted to sample the Pu–PuH_2 phase transition using a one-dimensional bias $\eta(N_H)$, where the order parameter is the number of hydrogens N_H, In the 3D Ising model, the spin up to spin down phase transition can be sampled using such a one-dimensional bias projected onto the number of up spins. However, we found that independent WL trials using $\eta(N_H)$ did not converge for the PuH_x spin-lattice model (see Fig. S4). This complexity arises because H atoms occupy T sites in PuH_2, consistent with experimental evidence regarding lanthanide-hydrides, but H atoms in δ-Pu
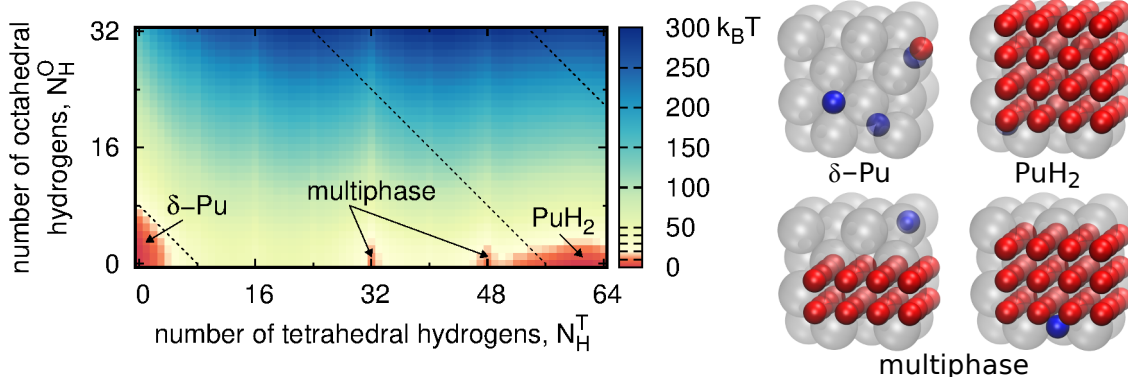
Figure 2: (Left) Two-dimensional free energy projected onto the number of hydrogen atoms in O sites N_H^O and in T sites N_H^T at 673 K for a system of $N_{Pu} = 32$ and reweighted to μ_{H2}^{equil} = -568.8 kJ/mol. Dashed lines show the boundaries of integration for determining μ_{H2}^{equil}. (Right) δ-Pu, PuH$_2$, and metastable multiphase configurations. The corresponding location of each configuration on the free energy surface is indicated by an arrow.

are most favorably bound in O sites. A simulation that employs a bias $\eta(N_H)$ and visits the δ-Pu basin will likely be biased towards configurations with more occupied O sites, a direction orthogonal to the Pu–PuH$_2$ transition, rather than toward configurations with more occupied T sites.

As a result, new configurations were generated via single spin flip Monte Carlo moves using a two-dimensional (2D) WL bias $\eta(N_H^O, N_H^T)$, where N_H^O is the number of occupied O sites and N_H^T is the number of occupied T sites. The negative of the converged bias is the free energy surface projected onto N_H^O and N_H^T. The δ-Pu phase corresponds to the free energy basin in the region $N_H/N_{Pu} \leq 0.25$, while the PuH$_2$ phase is the free energy basin within the region $1.75 \leq N_H/N_{Pu} \leq 2.7$. Four independent trials converged $\eta(N_H^O, N_H^T)$ to within 0.13 k_BT. The free energy surface of the Pu + H$_2$ $\rightleftharpoons$ PuH$_2$ reaction at 673 K and $N_{Pu} = 32$ is shown in Fig. 2, reweighted from an arbitrary μ_{H_2} = -615 kJ/mol to the equilibrium chemical potential $\mu_{H_2}^{equil}$, i.e., the chemical potential at which the integrated free energies of the δ-Pu and PuH$_2$ basins are equal. Due to periodic boundary conditions, multiphase configurations containing regions of δ-Pu and PuH$_2$ are also metastable for the $N_{Pu} = 32$ system. These are responsible for valleys in the free energy surface (see Fig. 2) at $N_H^T = 16$, 32, and 48 corresponding to one, two, or three filled layers of T sites. The

10

metastability of such configurations decreases with increasing system size (see Fig. S5-S9), but does not effect the calculation of μ_{H2}^{equil} as will be shown below.

The free energy surface in Fig. 2 required calculating the energy of over one billion configurations. Using our spin-lattice model, this required 29 hours on one Intel Broadwell processor (2.1 GHz). The required simulation time increased with decreasing temperature; simulations at 298 K required 8 days of computing time. In contast, a single point energy calculation with spin-polarized DFT and a GGA+U correction required 30 minutes on 216 of the same Intel processors. As a result, we estimate our model yields a computational speedup of a factor of $\mathcal{O}(10^7)$.

The effect of system size on the computed equilibrium chemical potential $\mu_{H_2}^{equil}$ was investigated using systems of $N_{Pu} = 4, 32, 108, 256$, and 500. One-dimensional free energy plots for each system are shown in Fig. 3a. The free energy barriers between phases decreases with increasing N_{Pu} until $N_{Pu} \geq 256$, indicating that systems of $N_{Pu} \leq 108$ under sample the configurational entropy of a growing δ-Pu or PuH_2 nucleus. However, the actual value of $\mu_{H_2}^{equil}$ is less sensitive to system size (see Fig. 3b). While $\mu_{H_2}^{equil}$ computed from the smallest system, $N_{Pu} = 4$, is 13.6 kJ/mol above that from the largest system, $N_{Pu} = 500$, the error from computing $\mu_{H_2}^{equil}$ for the $N_{Pu} = 32$ supercell is only $+0.8$ kJ/mol. Phase equilibrium at each temperature was therefore computed at the $N_{Pu} = 32$ system size for the sake of computational efficiency.

Free energies reweighted to $\mu_{H_2}^{equil}$ are shown in Fig. 4a for temperatures $T = 298, 373, 473,$ 573, 673, 723,$ and 773 K. The equilibrium pressures $P_{H_2}^{equil}$ are recovered from the $\mu_{H_2}^{equil}$ by modeling the hydrogen reservoir as an ideal gas of harmonically oscillating, rigidly rotating linear molecules (see Eqs. S5-S6). Experimental pressures for the temperatures 673–773 K are small, ranging from 1-37 Pa.[5,9,10] The simulated results for this same temperature range systematically overpredict the experimental pressures by a scaling factor of 5-8. This could be due to errors inherent in the exchange-correlation functional used to parameterize our model (PBE), as well as our simulation of perfect Pu and PuH_2 crystals. In particular, the
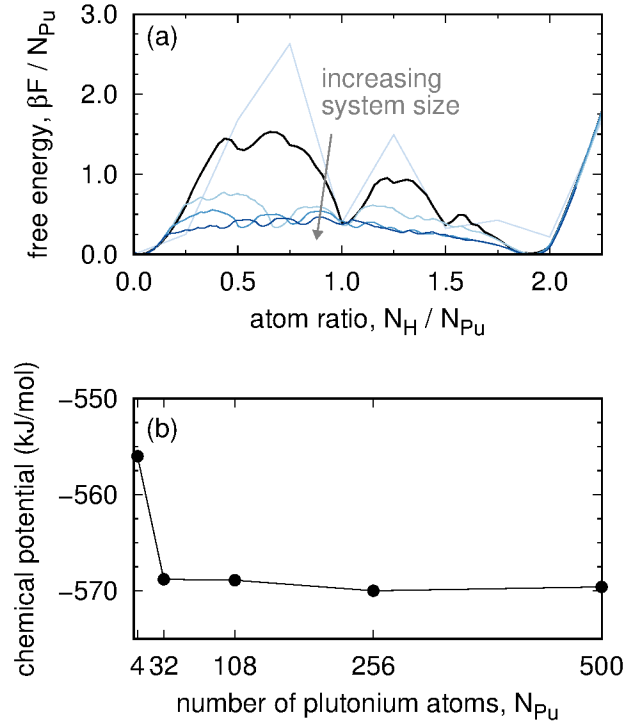
Figure 3: (a) Free energy projected onto the ratio of hydrogen-to-plutonium atoms at temperature 673 K for systems of $N_{Pu} = 4$, 32, 108, 256, 500 and reweighted to the equilibrium chemical potential. (b) The equilibrium chemical potential as a function of system size. Error bars are smaller than the symbol size.

lack of defects, impurities, and grain boundaries in our spin-lattice model, which could act as nucleation sites and thus allow for PuH_2 formation at lower pressures could be contributing to this discrepancy. Despite this systematic error, Fig. 4b shows that the simulated heat of formation, -140 kJ/mol, is within 7-16 kJ/mol of the experimental results, -147[9] to -156[5] kJ/mol. Our simulations confirm that the saturation pressure of δ-Pu becomes truly miniscule as temperature decreases. At room temperature, we predict the equilibrium pressure to be $\mathcal{O}(10^{-14})$ Pa.
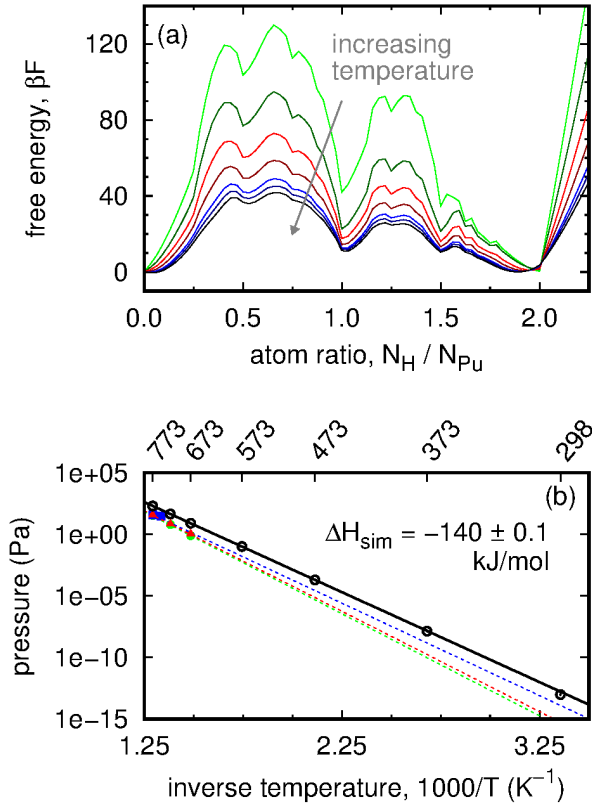

Figure 4: (a) Free energy projected onto the ratio of hydrogen-to-plutonium atoms for a system of $N_{Pu} = 32$ at temperatures 298, 373, 473, 573, 673, 723, 773 K and reweighted to the equilibrium chemical potential. (b) van't Hoff plot of equilibrium pressures from experiment (red triangles,[5] blue squares,[9] green filled circles[10]) and simulation (black open circles). Error bars on simulation data are smaller than the symbol size.

13

The average equilibrium compositions of each phase are compared to experimental values in Table 1. The hydrogen saturatation of δ-Pu and the number of T site vacancies in PuH_2 both increase with temperature. In addition, the simulated and experimental saturation composition of PuH_2 at 773 K are in excellent agreement. Mulford and Sturdy were unable to determine, on the basis of composition alone, whether the equilibrated PuH_2 was plutonium-rich (due to interstitial Pu atoms) or hydrogen-deficient.[5] While our results cannot eliminate the possibility that interstitial Pu contribute to the non-stoichiometric upper solubility limit, we can confirm that presence of T site vacancies is a sufficient descriptor.

Table 1: Equilibrium composition N_H/N_{Pu} of the δ-Pu and PuH_2 phases as a function of temperature, in K. Sampling uncertainties in simulated compositions are less than 0.0007.

| Temp | Pu | | | PuH_2 | |
	sim	Ref. 9[a]	Ref. 10[b]	sim	Ref. 5[c]
298	0.00114	$(10^{-9})^d$	–	1.989	–
373	0.00528	–	–	1.976	–
473	0.0142	–	–	1.950	–
573	0.0256	–	–	1.924	–
673	0.0371	–	0.012^e	1.904	–
723	0.0428	–	0.015^e	1.896	–
773	0.0486	0.00777	0.011^f	1.888	1.88

[a]Pu-2 wt.%-Ga
[b]Pu-2 at.%-Ga
[c]unalloyed Pu
[d]extrapolated exponentially from higher temperature data
[e]approximated visually
[f]linearly interpolated from data at 748 and 798 K

In general, our simulations over-predict the hydrogen saturation of δ-Pu by a factor of 3-6 compared to experimental values. This discrepancy is unlikely to be due to the presence of gallium in the experimental alloys, since Ga has been to shown to enhance the solubility of H in Pu.[10] Rather, it could be a consequence of our decision to limit H–H interactions in our model to nearest neighbor O sites. The binding of a H in one O site effectively blocks the 12 neighboring O sites from being occupied due to the high energy required to insert a hydrogen in those locations. Longer range H–H interactions could exclude additional

O sites for example, and would subsequently reduce the H solubility, relative to our model. Nevertheless, we predict similarly small hydrogen solubility in Pu under these conditions. Additionally, our model allows us to assess the room temperature solubility limit of δ-Pu more rigorously than the only prior effort, which was determined by extrapolating from an exponential fit to high temperature data[9] and thus could be error prone. For example, these results show a six order of magnitude decrease in hydrogen solubility of unalloyed plutonium over an approximate 500 K temperature decrease, whereas our simulations directly compute a decrease of only 1-2 orders of magnitude over the same temperature range.

Our spin-lattice approach accounts for H–H interactions in nearest neighbor O and T sites and leverages a tractable number of energies computed via DFT. This allows for the calculation of accurate Pu–PuH$_2$ phase envelopes at a fraction of the cost of standard quantum mechanical approaches. Our results yield quantitative agreement with experiment regarding the solubility limits of hydrogen in plutonium, and predict the heat of formation of PuH$_2$ to within 7-16 kJ/mol of the experimental range of results. Structurally, we confirm that hydrogen occupies available T sites in PuH$_2$ leaving nearly all O sites vacant, but show that hydrogen binds preferentially in O sites at low solubility. Efforts to model plutonium hydride nucleation and incorporate surface effects is the subject of future work. We anticipate that our spin-lattice model could be parameterized to examine the hydride phase envelopes of other fcc actinides, rare earth metals, or transition metals (e.g., thorium, cerium, and palladium). Overall, our predictions provide a baseline to guide future plutonium experiments and, more generally demonstrate the ability to access the length and time scales necessary to compute experimentally-verifiable quantities in solid state chemistry by coarse-grained models while retaining most of the accuracy of quantum calculations.

Acknowledgement

Supporting Information Available

The following files are available:

- Tabulated simulation results for each figure; additional details regarding the computational methods employed; additional figures showing two-dimensional free energies as a function of system size and temperature.

- Video, 1000 sweeps of grand canoncial simulations of hydrogen absorption at N_{Pu}=32, T=673 K, and μ_{H_2}=-568.8 kJ/mol of (left) an unbiased trajectory starting from δ-Pu, (center) an unbiased trajectory starting from PuH$_2$, (right) a Wang-Landau trajectory. Atoms are color-coded: Pu (gray), H in T sites (red), H in O sites (blue).

References

(1) https://en.wikipedia.org/wiki/Plutonium-238 (accessed Feb. 20, 2020).

(2) Ward, J. W.; Haschke, J. M. Comparison of 4f and 5f element hydride properties. *Handbook on the Physics and Chemistry of Rare Earths* **1994**, *18*, 293–363.

(3) Haschke, J.; Allen, T. H.; Morales, L. A. Surface and corrosion chemistry of plutonium. *Los Alamos Science* **2000**, *26*, 252–273.

(4) Manchester, F.; San-Martin, A.; Pitre, J. The H-Pd (hydrogen-palladium) system. *J. Phase Equilib.* **1994**, *15*, 62–83.

(5) Mulford, R. N.; Sturdy, G. E. The Plutonium-Hydrogen System. I. Plutonium Dihydride and Dideuteride1. *J. Am. Chem. Soc.* **1955**, *77*, 3449–3452.

(6) Arsenlis, A.; Wolfer, W.; Schwartz, A. Change in flow stress and ductility of δ-phase Pu–Ga alloys due to self-irradiation damage. *J. Nucl. Mater.* **2005**, *336*, 31–39.

(7) Worsham Jr, J.; Wilkinson, M.; Shull, C. Neutron-Diffraction Observations on the Palladium-hydrogen and Palladium-deuterium systems. *J. Phys. Chem. Solids* **1957**, *3*, 303–310.

(8) Fukai, Y. *The Metal-Hydrogen System: Basic Bulk Properties*; Springer Science & Business Media, 2006; Vol. 21.

(9) Allen, T. H. The solubility of hydrogen in plutonium in the temperature range 475 to 825 degrees centigrade. M.Sc. thesis, University of Colorado, 1991.

(10) Richmond, S.; Bridgewater, J. S.; Ward, J. W.; Allen, T. H. The solubility of hydrogen and deuterium in alloyed, unalloyed and impure plutonium metal. *IOP Conf. Ser. Mater. Sci. Eng.* **2010**, *9*, 012036.

(11) Savrasov, S. Y.; Kotliar, G.; Abrahams, E. Correlated electrons in δ-plutonium within a dynamical mean-field picture. *Nature* **2001**, *410*, 793.

(12) Söderlind, P.; Landa, A.; Sadigh, B. Density-functional investigation of magnetism in δ-Pu. *Phys. Rev. B* **2002**, *66*, 205109.

(13) Söderlind, P.; Sadigh, B. Density-Functional Calculations of α, β, γ, δ, δ', and ϵ Plutonium. *Phys. Rev. Lett.* **2004**, *92*, 185702.

(14) Söderlind, P. Quantifying the importance of orbital over spin correlations in δ- Pu within density-functional theory. *Phys. Rev. B* **2008**, *77*, 085101.

(15) Liu, T.; Cai, T.; Gao, T.; Li, G. The electronic and structural properties of δ-Pu and PuO from the LSDA (GGA)+ U method. *Physica B* **2010**, *405*, 3717–3721.

(16) Söderlind, P.; Zhou, F.; Landa, A.; Klepeis, J. Phonon and magnetic structure in δ-plutonium from density-functional theory. *Sci. Rep.* **2015**, *5*, 15958.

(17) Migliori, A.; Söderlind, P.; Landa, A.; Freibert, F. J.; Maiorov, B.; Ramshaw, B.; Betts, J. B. Origin of the multiple configurations that drive the response of δ-plutonium's elastic moduli to temperature. *P. Natl. Acad. Sci.* **2016**, *113*, 11158–11161.

(18) Goldman, N.; Morales, M. A. A First-Principles Study of Hydrogen Diffusivity and Dissociation on δ-Pu (100) and (111) Surfaces. *J. Phys. Chem. C* **2017**, *121*, 17950–17957.

(19) Ao, B.; Wang, X.; Shi, P.; Chen, P.; Ye, X.; Lai, X.; Gao, T. First-principles LDA+ U calculations investigating the lattice contraction of face-centered cubic Pu hydrides. *J. Nucl. Mater.* **2012**, *424*, 183–189.

(20) Yong, G.; Juan-Juan, A.; Tao, G.; Bing-Yun, A. Structural, magnetic, electronic, and elastic properties of face-centered cubic PuHx (x= 2, 3): GGA (LSDA)+ U+ SO. *Chin. Phys. B* **2013**, *22*, 057103.

(21) Zheng, J.-J.; Wang, B.-T.; Di Marco, I.; Li, W.-D. Electronic structure and phase stability of plutonium hydrides: Role of Coulomb repulsion and spin-orbital coupling. *Int. J. Hydrog. Energy* **2014**, *39*, 13255–13265.

(22) Yang, Y.; Zhang, P. Hydriding and dehydriding energies of PuHx from ab initio calculations. *Phys. Lett. A* **2015**, *379*, 1649–1653.

(23) Torrie, G. M.; Valleau, J. P. Nonphysical sampling distributions in Monte Carlo free-energy estimation: Umbrella sampling. *J. Comput. Phys.* **1977**, *23*, 187–199.

(24) Zwanzig, R. W. High-temperature equation of state by a perturbation method. I. Non-polar gases. *J. Chem. Phys.* **1954**, *22*, 1420–1426.

(25) Aqvist, J. Ion-water interaction potentials derived from free energy perturbation simulations. *J. Phys. Chem.* **1990**, *94*, 8021–8024.

(26) Shirts, M. R.; Mobley, D. L.; Chodera, J. D. Alchemical free energy calculations: ready for prime time? *Ann. Rep. Comput. Chem.* **2007**, *3*, 41–59.

(27) Darve, E.; Rodríguez-Gómez, D.; Pohorille, A. Adaptive biasing force method for scalar and vector free energy calculations. *J. Chem. Phys.* **2008**, *128*, 144120.

(28) Wang, F.; Landau, D. Efficient, multiple-range random walk algorithm to calculate the density of states. *Physical review letters* **2001**, *86*, 2050.

(29) Laio, A.; Parrinello, M. Escaping free-energy minima. *P. Natl. Acad. Sci.* **2002**, *99*, 12562–12566.

(30) Goldman, N.; Aradi, B.; Lindsey, R. K.; Fried, L. E. Development of a Multicenter Density Functional Tight Binding Model for Plutonium Surface Hydriding. *J. Chem. Theory Comput.* **2018**, *14*, 2652–2660.

(31) van de Walle, A.; Asta, M. D.; Ceder, G. The Alloy Theoretic Automated Toolkit: A User Guide. *Calphad* **2002**, *26*, 539–553.

(32) van de Walle, A. Multicomponent multisublattice alloys, nonconfigurational entropy and other additions to the Alloy Theoretic Automated Toolkit. *Calphad* **2009**, *33*, 266–278.

(33) Kamakoti, P.; Sholl, D. S. Ab initio lattice-gas modeling of interstitial hydrogen diffusion in CuPd alloys. *Phys. Rev. B* **2005**, *71*, 014301.

(34) Sonwane, C. G.; Wilcox, J.; Ma, Y. H. Solubility of hydrogen in PdAg and PdAu binary alloys using density functional theory. *J. Phys. Chem. B* **2006**, *110*, 24549–24558.

(35) Sonwane, C. G.; Wilcox, J.; Ma, Y. H. Achieving optimum hydrogen permeability in PdAg and PdAu alloys. *J. Chem. Phys.* **2006**, *125*, 184714.

(36) Semidey-Flecha, L.; Sholl, D. S. Combining density functional theory and cluster expansion methods to predict H 2 permeance through Pd-based binary alloy membranes. *J. Chem. Phys.* **2008**, *128*, 144701.

(37) Semidey-Flecha, L.; Ling, C.; Sholl, D. S. Detailed first-principles models of hydrogen permeation through PdCu-based ternary alloys. *J. Membrane Sci.* **2010**, *362*, 384–392.

(38) Keita, N. Lattice model simulation of hydrogen effect on palladium gold alloys used as purification metal membranes. Ph.D. thesis, Georgia Institute of Technology, 2012.

(39) Tafen, D. N. First-principles-based kinetic Monte Carlo studies of diffusion of hydrogen in Ni–Al and Ni–Fe binary alloys. *J. Mater. Sci.* **2015**, *50*, 3361–3370.

(40) Kaufman, L.; Cohen, M. Thermodynamics and kinetics of martensitic transformations. *Progress in Metal Physics* **1958**, *7*, 165–246.

(41) Wonczak, S.; Strey, R.; Stauffer, D. Confirmation of classical nucleation theory by Monte Carlo simulations in the 3-dimensional Ising model at low temperature. *J. Chem. Phys.* **2000**, *113*, 1976–1980.

(42) Kresse, G.; Hafner, J. Ab initio molecular dynamics for liquid metals. *Phys. Rev. B* **1993**, *47*, 558.

(43) Kresse, G.; Hafner, J. Ab initio molecular-dynamics simulation of the liquid-metal–amorphous-semiconductor transition in germanium. *Phys. Rev. B* **1994**, *49*, 14251.

(44) Kresse, G.; Furthmüller, J. Efficient iterative schemes for ab initio total-energy calculations using a plane-wave basis set. *Phys. Rev. B* **1996**, *54*, 11169.

(45) Dudarev, S.; Botton, G.; Savrasov, S.; Humphreys, C.; Sutton, A. Electron-energy-loss spectra and the structural stability of nickel oxide: An LSDA+ U study. *Phys. Rev. B* **1998**, *57*, 1505.